ACS APPLIED MATERIALS & INTERFACES

Research Article

Cite This: ACS Appl. Mater. Interfaces 2018, 10, 3341−3348

www.acsami.org

High-Precision Photothermal Ablation Using Biocompatible Palladium Nanoparticles and Laser Scanning Microscopy

Belén Rubio-Ruiz,[†,#] Ana M. Pérez-López,[†,#] Thomas L. Bray,[†] Martin Lee,[†] Alan Serrels,[‡] Martín Prieto,[⊥] Manuel Arruebo,[⊥,¶] Neil O. Carragher,[†] Víctor Sebastián,[⊥,¶] and Asier Unciti-Broceta*[,†]

[†]Cancer Research UK Edinburgh Centre, MRC Institute of Genetics and Molecular Medicine, University of Edinburgh, Crewe Road South, Edinburgh EH4 2XR, United Kingdom

[‡]MRC Centre for Inflammation Research, Queen's Medical Research Institute, University of Edinburgh, Edinburgh EH16 4TJ, United Kingdom

[⊥]Department of Chemical Engineering, Aragon Institute of Nanoscience (INA), University of Zaragoza, Campus Río Ebro-Edificio I+D, c/Poeta Mariano Esquillor s/n, 50018 Zaragoza, Spain

[¶]Networking Research Center on Bioengineering, Biomaterials and Nanomedicine (CIBER-BBN), 28029 Madrid, Spain

Supporting Information

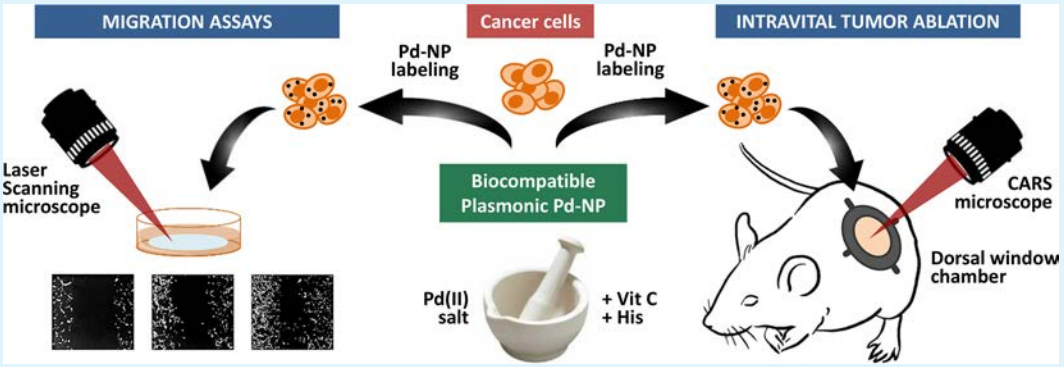

ABSTRACT: Herein, we report a straightforward method for the scalable preparation of Pd nanoparticles (Pd-NPs) with reduced inherent cytotoxicity and high photothermal conversion capacity. These Pd-NPs are rapidly taken up by cells and able to kill labeled cancer cells upon short exposure to near-infrared (NIR) light. Following cell treatment with Pd-NPs, ablated areas were patterned with high precision by laser scanning microscopy, allowing one to perform cell migration assays with unprecedented accuracy. Using coherent Raman microscopy, cells containing Pd-NPs were simultaneously ablated and imaged. This novel methodology was combined with intravital imaging to mediate microablation of cancerous tissue in tumor xenografts in mice.

KEYWORDS: *palladium, nanoparticles, photothermal effect, CARS, bioorthogonal, laser scanning microscopy*

INTRODUCTION

Photothermal ablation (PTA) is an optochemical method that employs benign electromagnetic radiations, preferably in the near-infrared region, to irradiate and kill cells (e.g., cancer cells) that have been pretargeted with photosensitive plasmonic materials.[1,2] Such materials, which typically consist of nontoxic cell-permeant nanostructures, release the absorbed energy as heat causing local hyperthermia and selectively disrupting the integrity of labeled cells. Plasmonic nanomaterials displaying photothermal activity under deep-penetrating NIR irradiation include various nanoarchitectures of noble metals (gold, silver, etc.), semiconductor quantum dots, and carbon-based nanomaterials (carbon nanotubes, graphene, organic nanoparticles).[1−4] While PTA is generally considered an extension of photodynamic therapy (PDT),[5] this "tag-&-kill" approach does not require oxygen to elicit its therapeutic action; a critical advantage for example for the prospective treatment of late stage hypoxic tumors. PTA together with PDT[5,6] and other emerging strategies, such as photopharmacology[7,8] and bioorthogonally activated prodrugs,[9−13] form a distinctive group of therapeutic approaches with the common feature of being "switched on" through bioindependent triggering stimuli, e.g., harmless electromagnetic waves, bioorthogonal partners, biocompatible catalysts, etc. The goal of these strategies is to minimize systemic adverse effects of cancer treatment by taking control of where and when the therapeutic intervention takes place.

Received: November 13, 2017
Accepted: January 10, 2018
Published: January 10, 2018

DOI: 10.1021/acsami.7b17282
ACS Appl. Mater. Interfaces 2018, 10, 3341−3348

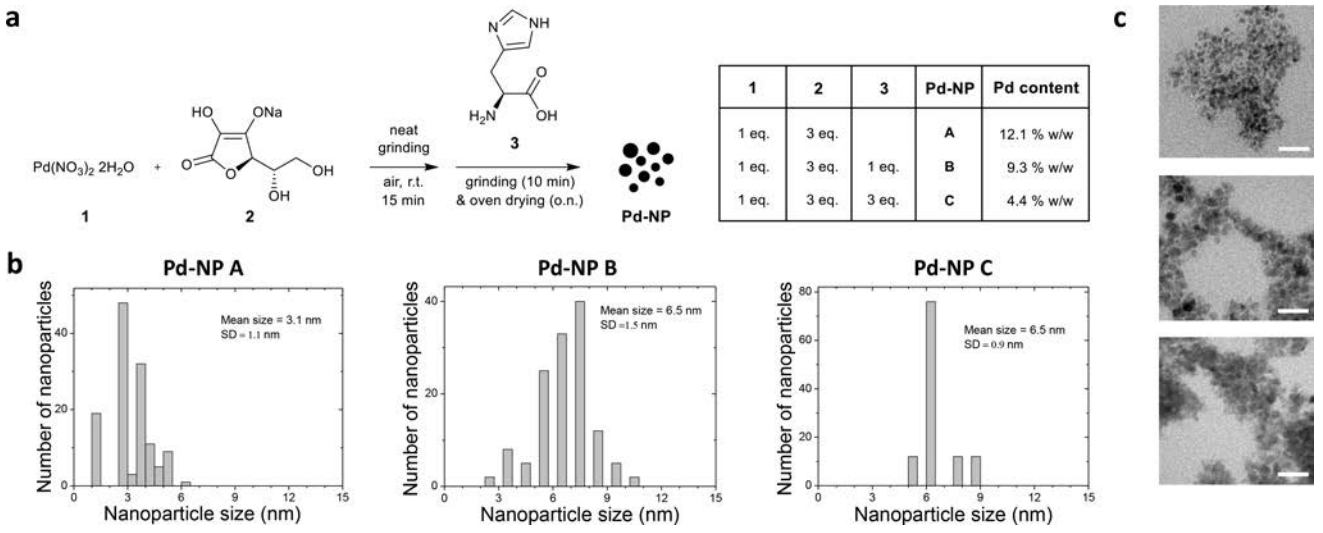

Figure 1. Green synthesis and characterization of Pd-NP. (a) Pd-NPs were prepared by neat grinding in a mortar using the recipe described in the table followed by oven drying at 80 °C. Pd content (w/w) was determined by inductively coupled plasma optical emission spectrometry (ICP-OES). (b) Size distribution histograms (≥150 particles measured per sample; SD = standard deviation) and (c) representative transmission electron microscopy (TEM) images of **Pd-NP A** (top), **B** (middle), and **C** (bottom). Histograms were generated by analysis of the TEM images.

Due to their remarkable chemical and optical properties, Pd nanostructures have recently emerged as a new player in the field of nanomedicine.[14,15] Polymer-entrapped Pd-NPs exhibit an exceptional capacity to elicit local bioorthogonal activation of different chemotherapeutic agents,[11,16−18] while Pd nanosheets and porous Pd-NPs facilitate the induction of local hyperthermia upon exposure to NIR irradiation.[19,20] Despite these encouraging studies, safety concerns associated with the potential toxicity and immunogenicity of Pd-NP in vivo[21−23] are deterring the advance of such technologies to the clinic. This has motivated efforts to develop Pd-based nanomaterials with high biocompatibility. Tilley and co-workers recently reported a method to deposit gold nanocrystals on highly branched Pd seeds as a way to increase the safety of the device and produce a NIR-absorbing composite nanostructure for photothermal therapy.[24] Other groups have exploited the natural reductant properties of plants and microbial extracts for the preparation of Pd-NPs (so-called biogenic synthesis),[25] which has resulted in the discovery of Pd-NPs with preferential ability to kill malignant cells over normal cells.[26,27]

Herein, we report a straightforward, scalable method to prepare Pd-NPs with high biocompatibility and plasmonic photothermal efficacy. These nanodevices enter cancer cells with high efficiency, remain in the cytoplasm without causing direct cell damage, and induce thermal ablation under harmless NIR laser irradiation. Using coherent Raman microscopy, ablation of Pd-labeled cells was ignited and simultaneously imaged in real-time both in vitro and in vivo. Cell labeling with Pd-NPs followed by laser microscopy-controlled irradiation enabled highly accurate patterning of denuded areas within a cell monolayer allowing the study of cancer cell migration and invasion with a level of accuracy that improves upon standard scratch wound healing assays.

RESULTS AND DISCUSSION

Rationale, Synthetic Procedure, and Characterization. Recent studies[26,27] have reported the use of natural extracts as biogenic reductants to produce Pd-NPs with preferential cytotoxic activity toward cancerous cells. Such selective properties might be, at least in part, a consequence of the combined action of bioactive substances present in the extracts being adsorbed at the NP surface.[28] Although this approach may be beneficial for the direct therapeutic use of such nanodevices, our goal was to develop an entirely biocompatible class of Pd-NPs to explore their bioorthogonal potential either to catalyze abiotic chemical processes[11,15] or to generate heat under harmless light irradiation.[14]

We envisioned that antioxidants and metal chelators found in human cells could be exploited to drive the reduction of soluble Pd(II) species into safe, well-characterized Pd-NPs. First, we tested four water-soluble natural antioxidants: ascorbate (vitamin C), uric acid, glutathione, and melatonin. Reactions were performed in water at 37 °C to mimic physiological conditions. As expected,[29−31] the addition of sodium ascorbate to a solution of palladium nitrate dihydrate ($Pd(NO_3)_2{\cdot}2H_2O$) led to the rapid generation of Pd-NPs, which was visually observed by a color change from brown to black. In contrast, glutathione and uric acid did not induce any color change to the mixture, indicating that Pd(II) is not reduced under such conditions. Interestingly, melatonin treatment at 37 °C for 6 h successfully reduced the Pd(II) salt into Pd^0. This is noteworthy as there are no references of the use of melatonin for the reduction of Pd(II) species. Unfortunately, instead of Pd-NPs, polydispersed microparticles were generated, making this method suboptimal for the purpose of this work. This novel green synthesis method of Pd powders may however find application in the microelectronics industry.[32]

Li and co-workers[31] have shown that sodium ascorbate can play a dual reductant/particle stabilizer role and generate Pd-NPs from different Pd(II) complexes in neat conditions by direct grinding in a mortar. Encouraged by the simplicity and scalability of this method, we adapted Li's protocol to prepare Pd-NP using $Pd(NO_3)_2{\cdot}2H_2O$ (**1**), sodium ascorbate (**2**), and histidine (**3**) (Figures 1a and S1). The natural amino acid **3** was used because of its high affinity to coordinate Pd atoms, its basic properties (the imidazole ring is partly protonated at physiological pH), and its antioxidant scavenging properties, especially against singlet oxygen[33] (one of the expected cytotoxic mechanisms attributed to Pd species[34]). We

DOI: 10.1021/acsami.7b17282
ACS Appl. Mater. Interfaces 2018, 10, 3341−3348

hypothesized that the adsorption of histidine molecules at the surface of the NPs would generate a positively charged layer at the periphery of the NPs to enhance intracellular delivery and partially neutralize the formation of Pd-mediated cell-damaging reactive oxygen species (ROS). This strategy would also help to decouple the photothermal from the photodynamic effect.

Three types of Pd-NP were prepared following the sequence described in Figure 1a (see full protocol in the Figure S1). On the basis of the amount of **3** used in the syntheses, Pd content (measured by ICP-OES) ranged from 12.1 wt % (**Pd-NP A**) to 4.4 wt % (**Pd-NP C**). TEM analysis showed that smaller nanoparticles were generated in the absence of histidine (**Pd-NP A**, mean size = 3.1 nm) in comparison to those containing the amino acid (**Pd-NP B** and **C**, mean sizes = 6.5 nm; see high resolution TEM in the Figure S2). X-ray powder diffraction (XRD) patterns (see Figure S3) showed the expected diffraction peaks attributed to Pd(0) and **2** in the three preparations. Signals confirming the presence of **3** in **Pd-NP B** and **C** were identified by XRD and Fourier-transform IR spectrometry (Figure S4).

Study of Pd-NP Biocompatibility and Intracellular Translocation. Chemicals containing Pd species are generally considered toxic.[35,36] Unbound Pd(II) complexes are reported to be poisonous,[36] while different types of Pd nanostructures have been shown to display cytotoxic activity against bacteria and cancer cells.[26,27,37] However, there is sufficient evidence to state that some Pd-containing materials are safer than others.[38,39] According to the European Medicines Evaluation Agency (EMEA), depending on the Pd reagent and the route of administration, median lethal dose values (LD_{50}) can drastically oscillate from 3 to 4900 mg/kg body weight,[39] evidencing that safety risks should not be generalized but evaluated in a case-by-case basis.

To determine whether the novel Pd-NPs were optimal for bioorthogonal applications, cell viability studies were carried out in human lung adenocarcinoma A549 cells. Cells were seeded in a 96-well plate and incubated for 48 h before treatment. Cells were then treated with increasing quantities of **Pd-NP A**, **B**, and **C** for 5 d, and cell viability was determined by the PrestoBlue assay. $Pd(NO_3)_2{\cdot}2H_2O$, **1**, was tested alongside as a control, and each experiment was performed in triplicates. Treatment with the Pd(II) salt **1** at 0.2 mg/mL led to complete cell death, whereas no signs of toxicity were observed at that concentration with the Pd-NPs. Notably, histidine-containing **Pd-NP B** and **C** exhibited a superior safety profile (Figure 2a). While compound **1** and **Pd-NP A** showed a drastic increase in cytotoxicity across a very narrow concentration range, the dose response curves of **Pd-NP B** and **C** displayed an attenuated slope. This reduced antiproliferative effect could be attributed to the ROS scavenging properties of histidine.[33]

Next, the capacity of the Pd-NPs to label lung cancer A549 cells was studied by measuring intracellular Pd content after 24 h of treatment. To ensure only internalized Pd-NPs were measured, cells were treated with 0.2 mg/mL of **Pd-NP A**, **B**, and **C** and then washed twice with PBS, trypsinized, and centrifuged. The supernatant was disposed, and the pellets were resuspended in the digestion solution and analyzed by ICP-OES. As shown in Figure 2b, Pd content in cells treated with **Pd-NP C** was negligible, which may explain their very low toxic effect on this cell line. Remarkably, the capacity of **Pd-NP B** to label A549 cells was over 3-fold higher than that of **Pd-NP A**. This is noteworthy because **Pd-NP B** contains a lower proportion of Pd in its structure than **Pd-NP A** and,

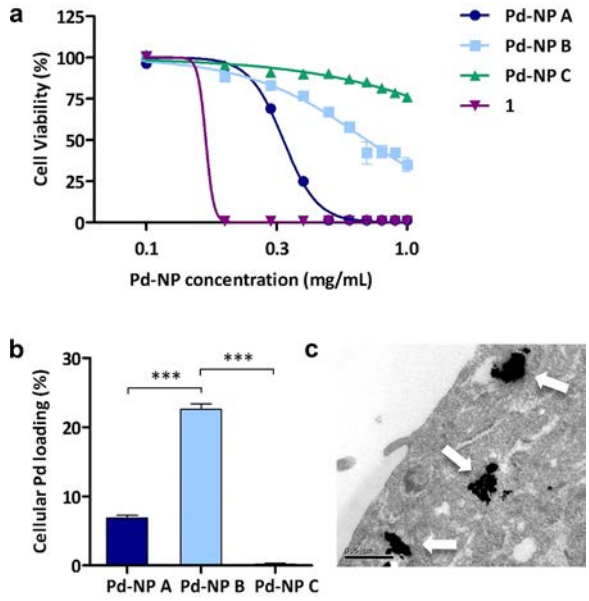

Figure 2. Cell viability and NP penetrability studies in A549 cells. (a) Dose response curves after treatment with **1**, **Pd-NP A**, **B**, and **C**. Cell viability was measured at day 5 using the PrestoBlue reagent. Error bars: ±SD from $n = 3$. (b) Quantification of Pd content inside cells as a percentage of the concentration used for the treatment. Analyses were performed by ICP-OES. (c) Representative Cryo-TEM image of a **Pd-NP B**-treated cell cross-section showing the membrane and the cytoplasm of a lung cancer A549 cell. NP clusters are indicated with white arrows. Scale bar = 500 nm. $***P \leq 0.001$.

importantly, **Pd-NP B** is also more biocompatible. To verify that **Pd-NP B** was able to enter the cell cytoplasm, rather than being adsorbed on the cell membrane, cells were treated with **Pd-NP B** following the same protocol described before. After labeling, detachment, and centrifugation, cells were resuspended in fresh media and replated over a sterile coverslip. Following 24 h of incubation, cells were fixed with paraformaldehyde and processed for Cryo-TEM analysis. TEM images confirmed the presence of **Pd-NP B** inside the cells, which appeared as clusters of various sizes across the cell cytoplasm (Figure 2c).

Analysis of the colloidal stability of each of the NPs in the presence of serum (see Figure S6) revealed that **Pd-NP B** produced particles of relatively stable size (approximately 200 nm in average diameter). On the contrary, the colloidal suspension generated by **Pd-NP C** under such conditions varied significantly over time, which may account for the low cell entry observed with **Pd-NP C** and, consequently, for its low cytotoxic effect.

Chemical and Optical Properties of Pd-NP A, B, and C: Absorbance and Photothermal Activity. After finding that **Pd-NP B** was optimal to label cancer cells and stay harmlessly in the cell cytoplasm, a series of in vitro functional studies were carried out to assess the capabilities of these nanodevices to perform bioorthogonal tasks.

On the basis of our interest in bioorthogonal organometallic (BOOM) chemistry,[40,41] the catalytic properties of **Pd-NP B** in biocompatible environments were evaluated using a selection of Pd-labile pro-dyes in PBS with and without 10% fetal bovine serum (FBS). While the nanodevices showed a high capacity to activate probes **4b** and **4c** in PBS, their catalytic activity in PBS supplemented with FBS was significantly lower (see Figure S7),

DOI: 10.1021/acsami.7b17282
ACS Appl. Mater. Interfaces 2018, 10, 3341−3348

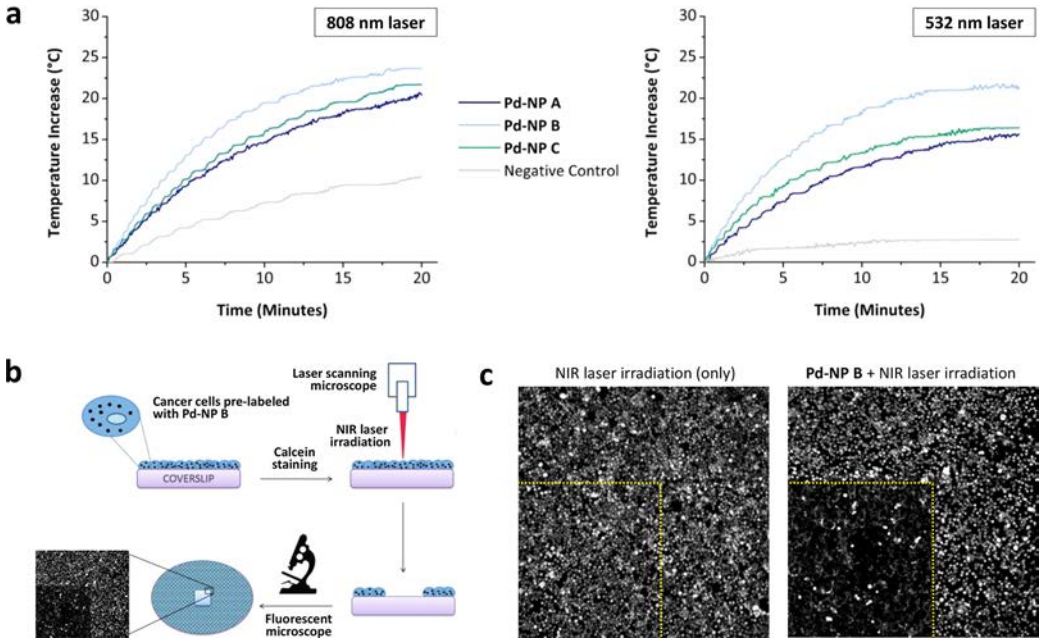

Figure 3. Analysis and applications of the plasmonic properties of **Pd-NP A**, **B**, and **C**. (a) Measurements of the variation of the temperature under laser irradiation (4 W/cm^2) for 20 min. (b) Protocol followed for the induction of PTA at precise areas of A549 cancer cell culture using laser scanning microscopy. (c) Fluorescent images (Ex/Em = 495/515 nm) of calcein AM-stained cancer cells after NIR laser irradiation: left panel, nonlabeled cells; right panel, cells labeled with **Pd-NP B**. Only areas within the yellow lines were irradiated using a laser scanning microscope.

indicating that these nanoparticles are deactivated by serum components and therefore not suitable to perform intracellular BOOM catalysis.

A remarkable feature of Pd nanostructures that has attracted the attention of the nanomedical field in recent years is their capacity to absorb light in the NIR range and transform it into heat, which has been used preclinically to mediate PTA of prelabeled cancer cells both in vitro and in vivo.[19,20] 0.2 mg/mL suspensions of **Pd-NP A**, **B**, and **C** in PBS were first analyzed with a spectrophotometer at 400−800 nm to assess the absorbance properties of the NPs across the UV−vis spectrum, with particular interest in the NIR. Notably, **Pd-NP B** and **C** (both of which contain histidine) displayed enhanced light absorbing properties, with the preparation of **Pd-NP B** exhibiting the highest absorbance (see Figure S8). This is an interesting observation as the total quantity of Pd metal in the preparations of **Pd-NP B** and **C** is lower than in that of **Pd-NP A**. As histidine does not absorb light on its own, this indicates that NP-bound histidine molecules are involved in the improved capacity of the materials to absorb light.

The photothermal properties of the suspensions were then analyzed under laser and light-emitting diode (LED) irradiation. Laser photothermal measurements were performed using a NIR laser system consisting of an 808 nm laser diode and with a green 532 nm laser diode (Changchun New Industries Optoelectronics Technology Co., China). Samples (0.2 mg/mL in water) were irradiated under magnetic stirring for 20 min. Temperature increase curves were registered using a type K thermocouple (RS Components, Corby, UK) immersed in the sample parallel to the path of the laser beam.[42] As shown in Figure 3a, irradiation of the preparations of **Pd-NP B** and **C** resulted in a higher temperature increase than that of **Pd-NP A**. These results correlate well with the superior absorbance of **Pd-NP B** and **C** at 800 nm (see Figure S8), which suggest that the use of histidine in the preparation of **Pd-NP B** and **C** increases NIR light absorption and, in turn, promotes their photothermal capabilities. The photothermal stability of **Pd-NP B** was confirmed by performing six successive irradiation cycles (see Figure S9).

As expected, analysis of changes in the temperature of the preparations under LED (noncoherent divergent beam) irradiation at 480 and 532 nm showed no or minimal effect at 0.53 W/cm^2 (see Figure S9), indicating that the devices should not inflict any damage to labeled cells under normal brightfield and fluorescence light during microscopy studies.

Laser Microscopy-Patterned PTA of Pd-Labeled Cancer Cell Culture. The induction of PTA of cancer cells tagged with plasmonic materials is typically performed in vitro by irradiating an external laser source onto a plate or coverslip containing the cells, resulting in a uniform laser exposure throughout the cell monolayer. Our goal, however, was to exploit the spatial accuracy and automated capabilities of laser scanning microscopes to illuminate specific areas of a cell monolayer with a focused NIR laser source. Irradiation of the specimen in an automated programmable manner would enable highly precise patterning of multiple samples with very high reproducibility. This was achieved following the methodology described in Figure 3b. Briefly, nonlabeled and **Pd-NP B**-labeled A549 cells were stained with Calcein AM immediately prior to irradiation. Calcein AM is a cell-penetrant pro-dye that becomes fluorescent (Ex/Em = 495/515 nm) after entering living cells. Designated areas of the cell culture plate were then exposed to irradiation from a picosecond pulsed 816.8 nm NIR laser using a 25× water immersion objective of a laser scanning microscope Olympus FV1000MPE. Areas of irradiation were scanned sequentially using a Prior H117 automated stage (9 × 9 square) with an exposure time of 20 s per position. The laser power measured after the objective was 30 mW. After irradiation, the specimens were imaged by standard fluorescent microscopy. As shown in Figure 3c, while both nonlabeled and Pd-labeled cells were irradiated with the same laser on the same area, only the specific area of **Pd-NP B**-labeled cells that was

DOI: 10.1021/acsami.7b17282
ACS Appl. Mater. Interfaces 2018, 10, 3341−3348

exposed to the laser displayed decreased fluorescence and damaged cells showing a complete loss of cell integrity, i.e., highly precise ablation of a predesignated area within the cell monolayer.

Laser Microscopy-Patterned Wound Healing Assay. Cell migration assays are essential to study physiological and pathological processes.[43−46] Among the number of assays available,[45] the in vitro scratch assay or wound healing assay[47] is probably the most widely used due to its reduced cost and simplicity. Traditional protocols generating scratch-wounds manually using pipette tips or a "rubber policeman" device are labor intensive and limited by significant issues with reliability and poor accuracy in the creation of equivalent scratches in width, and the resulting edges are typically irregular. While recent technologies (e.g., WoundMaker tool or the Oris cell migration assay) improve throughput and reproducibility, they are limited by the requirement for expensive device and monitoring equipment and also by the fixed position and width of a single wound. It would benefit the biomedical field enormously to have a simple method that could be accessible to most laboratories to perform customized cell migration studies with high accuracy and reliability across multiple cell culture devices and microtiter plate formats.

Encouraged by the simplicity of mapping out specific areas with scanning microscopy and the precise patterning achieved with the combination of **Pd-NP B**-tagged cells and laser microscopy-guided ablation, we decided to explore the potential of this method to establish customized cell migration assays with high accuracy. To this end, we used squamous cell carcinoma SSC-GFP cells, which constitutively express the green fluorescent protein (GFP) and therefore can be easily tracked using fluorescence microscopy.[48] This labeling strategy is further useful because, contrary to most chemical probes, proteins such as GFP denaturalize at high temperature and therefore the fluorescence would be conveniently switched off upon cell ablation.

Cells were first labeled with **Pd-NP B** using the procedure described before, followed by seeding in a 6-well glass bottom plate and incubation for 24 h. Areas of irradiation were scanned sequentially using an Olympus FV1000MPE (816.8 nm laser and 25× immersion objective lens) with a Prior H117 automated stage (9 × 1 line) with an exposure time of 10 s per position, resulting in a vertical line with the width of 500 μm. After patterning, the plate was introduced in an IncuCyte ZOOM device and images (fluorescent channel) were recorded every 2 h. As shown in Figure 4, a highly precise vertical line of ablated cells was observable from the samples that contained **Pd-NP B**-labeled cells at t = 0 (right panel), while no reduced cell viability was observed from the nonlabeled control (left panel). Time-lapse imaging enabled visual tracking and facile quantification of cells migrating into the wound with optimal accuracy and reliability.

Real-Time Cell Death and Imaging Using Coherent Raman Microscopy. Coherent anti-Stokes Raman scattering (CARS) microscopy is a type of fast-acquisition Raman microscopy[49] that uses the Raman active vibrational frequency of native chemical bonds present in biomolecules to produce image contrast. By coalignment of two incident laser beams at a particular frequency difference, CARS can be used, for example, to image lipids within tumors or to distinguish between normal and malignant cells without requiring cell components staining or expression of fluorescent-tagged proteins,[48] an effective

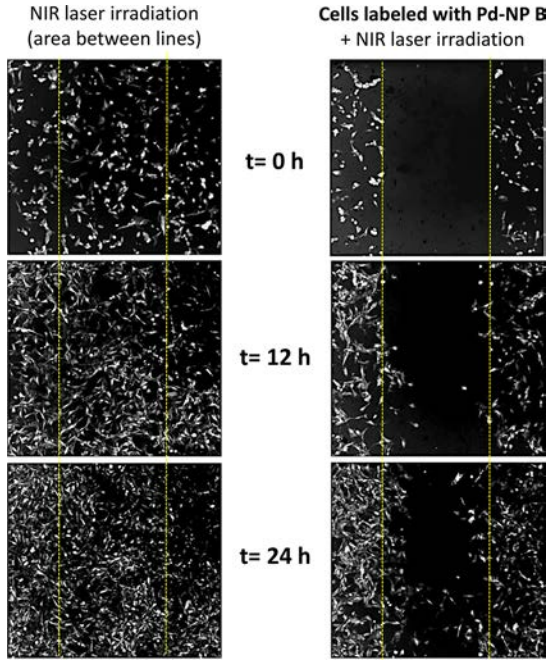

Figure 4. Laser microscopy-patterned wound healing assay with SCC-GFP cells at 0, 12, and 24 h after irradiation. Time-lapse imaging was performed using the green fluorescent channel of an IncuCyte ZOOM device.

solution for the label-free imaging of living cells and organisms with high spatial and temporal resolution.

Since the vibrational stimulation of aliphatic CH_2 groups is achieved with NIR lasers,[48] we envisaged that CARS microscopy could be used to kill and simultaneously image cancer cells labeled with plasmonic materials. To moderate the intensity of the photothermal effect and thereby facilitate the real-time visualization of the death of individual cells, A549 cancer cells were incubated with 0.02 mg/mL of **Pd-NP B** (10-fold lower concentration than that used in previous assays) following the protocol described above. Real-time movies were recorded by probing the CH_2 vibrational resonance with the lasers tuned to 816.8 and 1064.4 nm (30 and 20 mW, respectively) using a 25× water immersion objective of an Olympus FV1000MPE.

As observed at the center of the movie snapshots of Figure 5, the death of two cancer cells was clearly imaged. The cell pointed out with a yellow arrow appeared to die by necrosis, as indicated by its "bubbling" membrane in the mid panel (image at 237 s). This effect can be interpreted as membrane blebbing, which may be observed in both apoptotic cell death and necrosis. However, the high speed of the process (see Movie S1) suggests rapid necrotic cell injury. In contrast, the cell designated with a white arrow became progressively rounded without losing the integrity of the cell membrane, potentially suggesting programmed cell death. Such distinct effects are probably due to the induction of different degrees of intracellular hyperthermia, suggesting that the mode of death under a certain laser irradiation power would be dependent on the intracellular concentration of NPs within each particular cell. This is an important observation since the induction of apoptosis by photothermal therapy is believed to be advantageous for the treatment of cancer.[50] To the best of our knowledge, this is the first experiment showing that CARS microscopy can be used to image and kill cancer cells labeled

DOI: 10.1021/acsami.7b17282
ACS Appl. Mater. Interfaces 2018, 10, 3341−3348

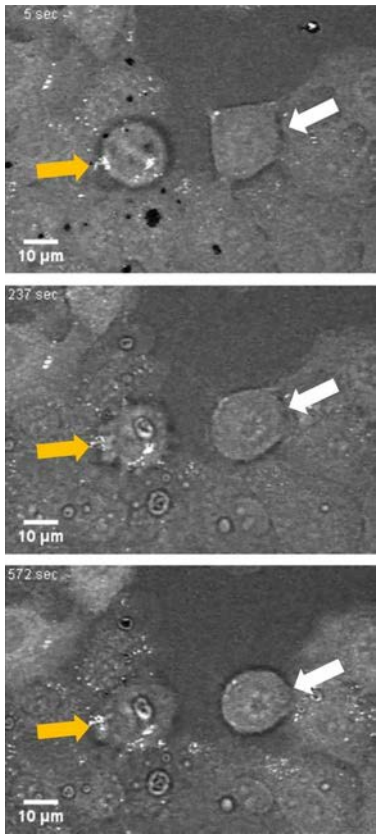

Figure 5. Snapshots of a real-time movie of **Pd-NP B**-labeled cancer cells under CARS stimulation. The yellow arrow indicates a cell dying by necrosis, and the white arrow points to a cell progressively changing its morphology into a rounded shape.

with plasmonic nanomaterials, a methodology that will be valuable for researchers working in the field of photothermal therapy.

In Vivo Xenograft Tissue Ablation Using Intravital Microscopy. The skin of the mouse is a physical barrier that impedes the direct visualization of subcutaneous tumor xenografts by confocal or multiphoton microscopy. To enable the study of the tumor microenvironment in vivo, researchers have developed optical window technologies that replace the mouse skin by a sterile glass coverslip.[51] These complex engineered devices facilitate high-resolution imaging of tumors in vivo at tissue, cellular, and subcellular levels to monitor tumor development or response to therapeutic treatments.[52] The recent introduction of CARS microscopy for intravital windows technology has expanded our capacity to visualize the tumor microenvironment without the need of fluorophores.[48] On the basis of the high biocompatibility, labeling capacity, and photothermal properties of **Pd-NP B**, we envisaged that we could generate Pd-labeled tumor xenografts that could be grown and, in turn, ablated in vivo using intravital CARS microscopy.

Dorsal window chambers were implanted into CD-1 nude mice as previously described.[53] A549 cells were labeled with **Pd-NP B** (0.2 mg/mL) following the procedure described above and implanted into the center of the window, and a glass coverslip was held in place using a circlip to seal the window. Xenografts of unlabeled cancer cells were used as negative control. Tumors were allowed to grow under the windows and then imaged under NIR irradiation by CARS microscopy at different areas on and outside of the tumor. Imaging/irradiation of the **Pd-NP**-labeled tumor tissue clearly revealed areas devoid of cells (Figure 6b, right panel) while, in contrast, the healthy (unlabeled) tissue of the same animal showed an intact physiology (Figure 6b, left panel). As previously reported,[48] intravital CARS imaging of a tumor xenograft composed of cancer cells without **Pd-NP B** showed no signs of cell ablation (see Figure S12). This proof-of-concept study demonstrates that the combination of CARS microscopy, intravital window technology, and biocompatible plasmonic nanomaterials can be applied to induce photothermal tissue ablation in designated areas of a tumor xenograft. While this method cannot be directly compared with standard PTA techniques (which typically employ optical fibers to irradiate large areas of xenografted malignancies), it could be used to induce and study in vivo microinjuries and, potentially, find application in precision medicine to treat superficial metastatic microlesions in combination with an appropriate tumor homing strategy (e.g., exploiting the enhanced permeability and retention (EPR) effect or incorporating cancer-targeting peptides on the surface of the NPs).

CONCLUSIONS

Highly biocompatible plasmonic Pd-NPs of around 6 nm in average diameter have been generated using a green, easily scalable synthetic procedure of high simplicity and reproducibility. Analysis of intracellular Pd content and TEM images demonstrated the capacity of one of the preparations (**Pd-NP**

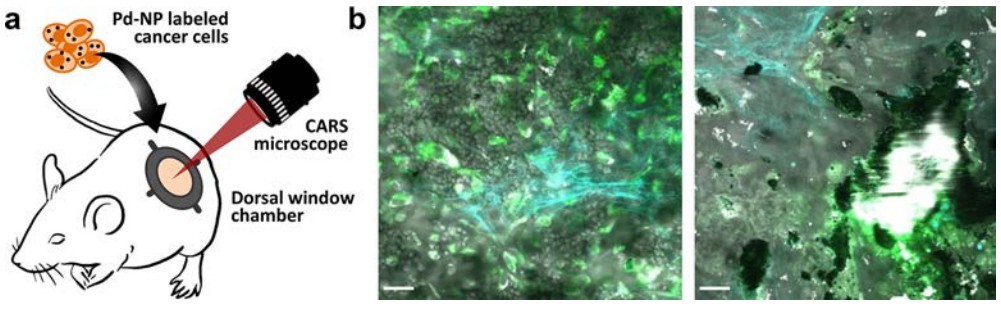

Figure 6. (a) In vivo xenograft tissue ablation using intravital CARS microscopy. Cancer cells were labeled with **Pd-NP B** before implantation. (b) Combined false color in vivo image of xenograft tissue. Images were generated using a CARS stimulation and filtered: nuclei (CH_3) in gray, cytoplasm (CH_2) in green, and collagen fibers (second harmonic generation) in cyan. Images were taken at the healthy tissue outside the A549 tumor (left panel) and at the center of the tumor (right panel). Ablated tissue areas are identified by dark openings of various sizes and shapes. Scale bars = 25 μm.

DOI: 10.1021/acsami.7b17282
ACS Appl. Mater. Interfaces 2018, 10, 3341−3348

B) to enter cancer cells and stay harmlessly in the cytoplasm. Notably, such NPs display high photothermal activity upon exposure to NIR laser irradiation. By labeling cancer cells with **Pd-NP B**, designated areas of cell culture specimens were precisely irradiated and ablated using a laser scanning microscope. Using this novel methodology, we developed an innovative wound healing assay that can be readily, and cost effectively, customized across multiple cell types and culture formats to facilitate more robust cell migration studies toward new applications and increased disease relevance. Finally, on the basis of the safety and optical properties of **Pd-NP B**, PTA studies were performed in combination with CARS microscopy both in vitro and in vivo, demonstrating the capacity of this method to "image & ignite" cell ablation in real time with high spatial precision. The concept of using CARS microscopy both to mediate and to monitor cell death in real time with robotic accuracy could open up new avenues to diversify the applicability of plasmonic materials in biomedical research and accelerate their clinical translation toward novel precision medicine initiatives against cancer.

■ ASSOCIATED CONTENT

Supporting Information

The Supporting Information is available free of charge on the ACS Publications website at DOI: 10.1021/acsami.7b17282.

Synthesis and characterization of materials, absorbance studies, photothermal studies, and biological methods (PDF)

Pd-NP B-labeled cancer cells under CARS stimulation (AVI)

■ AUTHOR INFORMATION

Corresponding Author

*E-mail: Asier.Unciti-Broceta@igmm.ed.ac.uk. Phone: 0044 131 6518500.

ORCID

Manuel Arruebo: 0000-0003-3165-0156

Víctor Sebastián: 0000-0002-6873-5244

Asier Unciti-Broceta: 0000-0003-1029-2855

Author Contributions

#B.R.-R. and A.M.P.-L. contributed equally.

Notes

The authors declare no competing financial interest.

■ ACKNOWLEDGMENTS

A.M.P.-L., N.O.C., and A.U.-B. are grateful to the EPSRC (EP/N021134/1) and the Royal Society (RG150377) for funding. B.R.-R. and T.L.B. thank the EC (H2020-MSCA-IF-2014-658833, ChemoBOOM) and the CMVM of the University of Edinburgh (Principal's scholarship), respectively, for financial support. M.L. and A.S. acknowledge the support of CRUK (C10195/A18075 and C157/A15703, respectively). M.A. and V.S. thank CIBER-BBN for financial support. CIBER-BBN is an initiative funded by the VI National R&D&i Plan 2008-2011 financed by the Instituto de Salud Carlos III with assistance from the European Regional Development Fund. V.S. is grateful to the University of Zaragoza (Project JIUZ-2016-TEC-13). M.A. also acknowledges the financial support of the ERC Consolidator Grant program (ERC-2013-CoG-614715). We acknowledge the support of the Wellcome Trust Multi User Equipment Grant (WT104915MA) for the TEM studies.

■ REFERENCES

(1) Jaque, D.; Martínez Maestro, L.; del Rosal, B.; Haro-Gonzalez, P.; Benayas, A.; Plaza, J. L.; Martín Rodríguez, E.; García Solé, J. Nanoparticles for photothermal therapies. *Nanoscale* **2014**, *6*, 9494−9530.

(2) Zou, L.; Wang, H.; He, B.; Zeng, L.; Tan, T.; Cao, H.; He, X.; Zhang, Z.; Guo, S.; Li, Y. Current Approaches of Photothermal Therapy in Treating Cancer Metastasis with Nanotherapeutics. *Theranostics* **2016**, *6*, 762−772.

(3) Abadeer, N. S.; Murphy, C. J. Recent Progress in Cancer Thermal Therapy Using Gold Nanoparticles. *J. Phys. Chem. C* **2016**, *120*, 4691−4716.

(4) Melamed, J. R.; Edelstein, R. S.; Day, E. S. Elucidating the fundamental mechanisms of cell death triggered by photothermal therapy. *ACS Nano* **2015**, *9*, 6−11.

(5) Lucky, S. S.; Soo, K. C.; Zhang, Y. Nanoparticles in photodynamic therapy. *Chem. Rev.* **2015**, *115*, 1990−2042.

(6) Dolmans, D. E.; Fukumura, D.; Jain, R. K. Photodynamic therapy for cancer. *Nat. Rev. Cancer* **2003**, *3*, 380−387.

(7) Velema, W. A.; Szymanski, W.; Feringa, B. L. Photopharmacology: beyond proof of principle. *J. Am. Chem. Soc.* **2014**, *136*, 2178−2191.

(8) Lerch, M. M.; Hansen, M. J.; van Dam, G. M.; Szymanski, W.; Feringa, B. L. Emerging Targets in Photopharmacology. *Angew. Chem., Int. Ed.* **2016**, *55*, 10978−10999.

(9) Reeßing, F.; Szymanski, W. Beyond Photodynamic Therapy: Light-Activated Cancer Chemotherapy. *Curr. Med. Chem.* **2017**, *24*, 4905−4950.

(10) Versteegen, R. M.; Rossin, R.; ten Hoeve, W.; Janssen, H. M.; Robillard, M. S. Click to release: instantaneous doxorubicin elimination upon tetrazine ligation. *Angew. Chem., Int. Ed.* **2013**, *52*, 14112−14116.

(11) Weiss, J. T.; Dawson, J. C.; Macleod, K. G.; Rybski, W.; Fraser, C.; Torres-Sánchez, C.; Patton, E. E.; Bradley, M.; Carragher, N. O.; Unciti-Broceta, A. Extracellular palladium-catalysed dealkylation of 5-fluoro-1-propargyl-uracil as a bioorthogonally activated prodrug approach. *Nat. Commun.* **2014**, *5*, 3277.

(12) Völker, T.; Dempwolff, F.; Graumann, P. L.; Meggers, E. Progress towards bioorthogonal catalysis with organometallic compounds. *Angew. Chem., Int. Ed.* **2014**, *53*, 10536−10540.

(13) Pérez-López, A. M.; Rubio-Ruiz, B.; Sebastián, V.; Hamilton, L.; Adam, C.; Bray, T. L.; Irusta, S.; Brennan, P. M.; Lloyd-Jones, G.; Sieger, D.; Santamaría, J.; Unciti-Broceta, A. Gold-Triggered Uncaging Chemistry in Living Systems. *Angew. Chem., Int. Ed.* **2017**, *56*, 12548−12552.

(14) Dumas, A.; Couvreur, P. Palladium: a future key player in the nanomedical field? *Chem. Sci.* **2015**, *6*, 2153−2157.

(15) Unciti-Broceta, A. Bioorthogonal catalysis: Rise of the nanobots. *Nat. Chem.* **2015**, *7*, 538−539.

(16) Weiss, J. T.; Dawson, J. C.; Fraser, C.; Rybski, W.; Torres-Sánchez, C.; Bradley, M.; Patton, E. E.; Carragher, N. O.; Unciti-Broceta, A. Development and bioorthogonal activation of palladium-labile prodrugs of gemcitabine. *J. Med. Chem.* **2014**, *57*, 5395−5404.

(17) Weiss, J. T.; Carragher, N. O.; Unciti-Broceta, A. Palladium-mediated dealkylation of N-propargyl-floxuridine as a bioorthogonal oxygen-independent prodrug strategy. *Sci. Rep.* **2015**, *5*, 9329.

(18) Rubio-Ruiz, B.; Weiss, J. T.; Unciti-Broceta, A. Efficient Palladium-Triggered Release of Vorinostat from a Bioorthogonal Precursor. *J. Med. Chem.* **2016**, *59*, 9974−9980.

(19) Huang, X.; Tang, S.; Mu, X.; Dai, Y.; Chen, G.; Zhou, Z.; Ruan, F.; Yang, Z.; Zheng, N. Freestanding palladium nanosheets with plasmonic and catalytic properties. *Nat. Nanotechnol.* **2011**, *6*, 28−32.

(20) Xiao, J. W.; Fan, S. X.; Wang, F.; Sun, L. D.; Zheng, X. Y.; Yan, C. H. Porous Pd nanoparticles with high photothermal conversion efficiency for efficient ablation of cancer cells. *Nanoscale* **2014**, *6*, 4345.

(21) Nel, A.; Xia, T.; Madler, L.; Li, N. Toxic potential of materials at the nanolevel. *Science* **2006**, *311*, 622−627.

(22) Fontana, L.; Leso, V.; Marinaccio, A.; Cenacchi, G.; Papa, V.; Leopold, K.; Schindl, R.; Bocca, B.; Alimonti, A.; Iavicoli, I. The effects

DOI: 10.1021/acsami.7b17282
ACS Appl. Mater. Interfaces 2018, 10, 3341−3348

of palladium nanoparticles on the renal function of female Wistar rats. *Nanotoxicology* **2015**, *9*, 843−851.
(23) Iavicoli, I.; Fontana, L.; Corbi, M.; Leso, V.; Marinaccio, A.; Leopold, K.; Schindl, R.; Sgambato, A. Exposure to Palladium Nanoparticles Affects Serum Levels of Cytokines in Female Wistar Rats. *PLoS One* **2015**, *10*, e0143801.
(24) McGrath, J.; Chien, Y. H.; Cheong, S.; Herman, D. A.; Watt, J.; Henning, A. M.; Gloag, L.; Yeh, C. S.; Tilley, R. D. Gold over Branched Palladium Nanostructures for Photothermal Cancer Therapy. *ACS Nano* **2015**, *9*, 12283−12291.
(25) Siddiqi, S.; Husen, A. Green Synthesis, Characterization and Uses of Palladium/Platinum Nanoparticles. *Nanoscale Res. Lett.* **2016**, *11*, 482.
(26) Gurunathan, S.; Kim, E.; Han, J. W.; Park, J. H.; Kim, J. H. 26. Green Chemistry Approach for Synthesis of Effective Anticancer Palladium Nanoparticles. *Molecules* **2015**, *20*, 22476−22498.
(27) Anand, K.; Tiloke, C.; Phulukdaree, A.; Ranjan, B.; Chuturgoon, A.; Singh, S.; Gengan, R. M. Biosynthesis of palladium nanoparticles by using Moringa oleifera flower extract and their catalytic and biological properties. *J. Photochem. Photobiol., B* **2016**, *165*, 87−95.
(28) Metz, M.; Sanders, S. E.; Pender, J. P.; Dix, M. R.; Hinds, D. T.; Quinn, S. J.; Ward, A. D.; Duffy, P.; Cullen, R. J.; Colavita, P. E. Green Synthesis of Metal Nanoparticles via Natural Extracts: The Biogenic Nanoparticle Corona and Its Effects on Reactivity. *ACS Sustainable Chem. Eng.* **2015**, *3*, 1610−1617.
(29) He, F.; Liu, J.; Roberts, C. B.; Zhao, D. One-Step "Green" Synthesis of Pd Nanoparticles of Controlled Size and Their Catalytic Activity for Trichloroethene Hydrodechlorination. *Ind. Eng. Chem. Res.* **2009**, *48*, 6550−6557.
(30) Castegnaro, V.; Kilian, A. S.; Baibich, I. M.; Alves, M. C.; Morais, J. On the reactivity of carbon supported Pd nanoparticles during NO reduction: unraveling a metal-support redox interaction. *Langmuir* **2013**, *29*, 7125−7133.
(31) Zhang, A.; Liu, M.; Liu, M.; Xiao, Y.; Li, Z.; Chen, J.; Sun, Y.; Zhao, J.; Fang, S.; Jia, D.; Li, F. Homogeneous Pd nanoparticles produced in direct reactions: green synthesis, formation mechanism and catalysis properties. *J. Mater. Chem. A* **2014**, *2*, 1369−1374.
(32) Ferrier, G. G.; Berzins, A. R.; Davey, N. M. The Production of Palladium Powders for Electronic Applications. *Platinum Metals Rev.* **1985**, *29*, 175−179.
(33) Matheson, B. C.; Etheridge, R. D.; Kratowich, N. R.; Lee, J. The quenching of singlet oxygen by amino acids and proteins. *Photochem. Photobiol.* **1975**, *21*, 165−171.
(34) Long, R.; Mao, K.; Ye, X.; Yan, W.; Huang, Y.; Wang, J.; Fu, Y.; Wang, X.; Wu, X.; Xie, Y.; Xiong, Y. Surface facet of palladium nanocrystals: a key parameter to the activation of molecular oxygen for organic catalysis and cancer treatment. *J. Am. Chem. Soc.* **2013**, *135*, 3200−3207.
(35) *Environmental Health Criteria 226: Palladium*; World Health Organization: Geneva, 2002.
(36) Hosseini, M. J.; Jafarian, I.; Farahani, S.; Khodadadi, R.; Tagavi, S. H.; Naserzadeh, P.; Mohammadi-Bardbori, A.; Arghavanifard, N. New mechanistic approach of inorganic palladium toxicity: impairment in mitochondrial electron transfer. *Metallomics* **2016**, *8*, 252−259.
(37) Balbín, A.; Gaballo, F.; Ceballos-Torres, J.; Prashar, S.; Fajardo, M.; Kaluđerović, G. N.; Gómez-Ruiz, S. Dual application of Pd nanoparticles supported on mesoporous silica SBA-15 and MSU-2: supported catalysts for C−C coupling reactions and cytotoxic agents against human cancer cell lines. *RSC Adv.* **2014**, *4*, 54775−54787.
(38) Egorova, S.; Ananikov, V. P. Which Metals are Green for Catalysis? Comparison of the Toxicities of Ni, Cu, Fe, Pd, Pt, Rh, and Au Salts. *Angew. Chem., Int. Ed.* **2016**, *55*, 12150−12162.
(39) European Medicines Agency. *Doc. Ref. CPMP/SWP/QWP/4446/00 corr.*; EMEA: London, 2007.
(40) Yusop, R. M.; Unciti-Broceta, A.; Johansson, E. M. V.; Sánchez-Martín, R. M.; Bradley, M. Palladium-mediated intracellular chemistry. *Nat. Chem.* **2011**, *3*, 239−243.
(41) Unciti-Broceta, A.; Johansson, E. M. V.; Yusop, R. M.; Sánchez-Martín, R. M.; Bradley, M. Synthesis of polystyrene microspheres and functionalization with Pd(0) nanoparticles to perform bioorthogonal organometallic chemistry in living cells. *Nat. Protoc.* **2012**, *7*, 1207−1218.
(42) Ortiz de Solorzano, I.; Prieto, M.; Mendoza, G.; Alejo, T.; Irusta, S.; Sebastian, V.; Arruebo, M. Microfluidic Synthesis and Biological Evaluation of Photothermal Biodegradable Copper Sulfide Nanoparticles. *ACS Appl. Mater. Interfaces* **2016**, *8*, 21545−21554.
(43) Carragher, N. O.; Frame, M. C. Modelling distinct modes of tumour invasion and metastasis. *Drug Discovery Today: Dis. Models* **2011**, *8*, 103−112.
(44) Warchal, S. J.; Unciti-Broceta, A.; Carragher, N. O. Next-generation phenotypic screening. *Future Med. Chem.* **2016**, *8*, 1331−1347.
(45) Kramer, N.; Walzl, A.; Unger, C.; Rosner, M.; Krupitza, G.; Hengstschläger, M.; Dolznig, H. In vitro cell migration and invasion assays. *Mutat. Res., Rev. Mutat. Res.* **2013**, *752*, 10−24.
(46) Fraser, C.; Dawson, J. C.; Dowling, R.; Houston, D. R.; Weiss, J. T.; Munro, A. F.; Muir, M.; Harrington, L.; Webster, S. P.; Frame, M. C.; Brunton, V. G.; Patton, E. E.; Carragher, N. O.; Unciti-Broceta, A. Rapid Discovery and Structure-Activity Relationships of Pyrazolopyrimidines That Potently Suppress Breast Cancer Cell Growth via SRC Kinase Inhibition with Exceptional Selectivity over ABL Kinase. *J. Med. Chem.* **2016**, *59*, 4697−4710.
(47) Liang, C.; Park, A. Y.; Guan, J. L. In vitro scratch assay: a convenient and inexpensive method for analysis of cell migration in vitro. *Nat. Protoc.* **2007**, *2*, 329−333.
(48) Lee, M.; Downes, A.; Chau, Y. Y.; Serrels, B.; Hastie, N.; Elfick, A.; Brunton, V.; Frame, M.; Serrels, A. In vivo imaging of the tumor and its associated microenvironment using combined CARS/2-photon microscopy. *IntraVital* **2015**, *4*, e1055430.
(49) Tipping, W. J.; Lee, M.; Serrels, A.; Brunton, V. G.; Hulme, A. N. Stimulated Raman scattering microscopy: an emerging tool for drug discovery. *Chem. Soc. Rev.* **2016**, *45*, 2075−2089.
(50) Melamed, R.; Edelstein, R. S.; Day, E. S. Elucidating the Fundamental Mechanisms of Cell Death Triggered by Photothermal Therapy. *ACS Nano* **2015**, *9*, 6−11.
(51) Serrels, A.; Canel, M.; Brunton, V. G.; Frame, M. C. Src/FAK-mediated regulation of E-cadherin as a mechanism for controlling collective cell movement. *Cell Adhesion & Migration* **2011**, *5*, 360−365.
(52) Conway, J. R.; Carragher, N. O.; Timpson, P. Developments in preclinical cancer imaging: innovating the discovery of therapeutics. *Nat. Rev. Cancer* **2014**, *14*, 314−328.
(53) Canel, M.; Serrels, A.; Miller, D.; Timpson, P.; Serrels, B.; Frame, M. C.; Brunton, V. G. Quantitative in vivo imaging of the effects of inhibiting integrin signaling via Src and FAK on cancer cell movement: effects on E-cadherin dynamics. *Cancer Res.* **2010**, *70*, 9413−9422.

DOI: 10.1021/acsami.7b17282
ACS Appl. Mater. Interfaces 2018, 10, 3341−3348